

New CDM Crisis Revealed by Multi-Scale Cluster Lensing

PRIYAMVADA NATARAJAN,^{1,2} BARRY T. CHIANG,¹ AND ISAQUE DUTRA²¹*Department of Astronomy, Yale University, New Haven, CT 06511, USA*²*Department of Physics, Yale University, New Haven, CT 06511, USA*

ABSTRACT

The properties of substructure in galaxy clusters, exquisitely probed by gravitational lensing, offer a stringent test of dark matter models. Combining strong and weak lensing data for massive clusters, we map their total mass—dominated by dark matter—over the dynamic range needed to confront small-scale predictions for collisionless cold dark matter (CDM). Using state-of-the-art lens models, we extract four key subhalo properties: the mass function, projected radial distribution, internal density profile, and tidal truncation radius. We find that the subhalo mass function and truncation radii are consistent with CDM expectations. In contrast, the inner density profiles and radial distribution of subhalos are strongly discrepant with CDM. The incidence of galaxy-galaxy strong lensing (GGSL) from subhalo cores exceeds CDM predictions by nearly an order of magnitude, requiring inner density slopes as steep as $\gamma \gtrsim 2.5$ within $r \lesssim 0.01 R_{200}$ consistent with core-collapsed self-interacting dark matter (SIDM), while the same subhalos behave as collisionless in their outskirts. Additionally, the observed radial distribution of subhalos hosting bright cluster member galaxies, explicitly modeled in the lens reconstructions, remains incompatible with CDM. Together, these small-scale stress tests reveal an intriguing paradox and challenge the dark matter microphysics of purely collisionless CDM and motivate hybrid scenarios, such as a dual-component model with both CDM and SIDM, or entirely new classes of dark matter theories.

Keywords: dark matter — galaxies: clusters: general — gravitational lensing: strong

1. INTRODUCTION

The Λ CDM paradigm excels in accounting for observations on large scales, matching data from the cosmic microwave background (CMB), baryon acoustic oscillations, and the derived matter power spectrum; however, persistent small-scale tensions remain (Del Popolo & Le Delliou 2017). Many of these tensions, including abundance mis-matches, for instance, with the missing satellites problem, and internal structure issues with the density profile shape leading to the cusp-core problem and the dwarf galaxy diversity problem have also been largely resolved with more sophisticated and improved simulation suites (Bullock & Boylan-Kolchin 2017; Sales et al. 2022; Cruz et al. 2025; Chiang et al. 2025b).

However, a particularly sharp and now data-rich challenge arises in massive cluster lenses: subhalos look CDM-like at large radii, while their inner regions serve

as far more efficient lenses predicted by state-of-the-art hydrodynamical simulations (Meneghetti et al. 2020a, 2022, 2023; Tokayer et al. 2024; Dutra et al. 2025; Chiang et al. 2025a). Lensing mass models generated and calibrated with observational data provide constraints on the total mass enclosed within subhalos but are unable to constrain at with current data quality, and are therefore agnostic to, how the mass may be distributed internally. Given this freedom, we are able to ray-trace through a range of assumed inner density profile slopes to reproduce the observed GGSL probabilities. This exercise requires extremely steep inner slopes r^γ ; with $\gamma \gtrsim 2.5$ inside $r \lesssim 10$ kpc (Dutra et al. 2025) even as truncation radii and outskirts remain NFW-like (Chiang et al. 2025a). The explicit contribution of baryons in the inner regions helps but appears insufficient to close the gap on their own (Tokayer et al. 2024).

There has been a long tradition of comparing the properties of lensing clusters and their substructure with CDM simulations; however, given their rarity and high-masses, it has been challenging to find mass-

matched simulated samples for cluster-lenses (Natarajan & Springel 2004; Natarajan et al. 2007, 2017a). With the availability of TNG-Cluster (TNG-C hereafter; Nelson et al. 2024) which resimulates ~ 350 clusters drawn from an extremely large, 1 Gpc^3 volume (thirty-six times larger than previous state-of-the-art TNG300 simulation box) is transformative for comparing detailed substructure properties. TNG-C is the first simulation suite that provides apt mass-matched samples for comparison with observed massive lensing clusters over cosmic time. In this work, we confront substructure properties derived from observed cluster lenses with those derived from mass-matched CDM cluster analogs from the TNG-C simulations.

The outline of this Letter is as follows: we first describe the observed cluster sample (Section 2) and lens model construction methodology (Section 3), and the properties of the corresponding simulated cluster analogs (Section 4). Next, we compare each of the following diagnostics of the observed substructure properties against theoretical predictions from simulated CDM analogs in TNG-C: the subhalo mass functions (Section 5), projected radial distributions (Section 6), inner density profiles (Section 7), and outer truncation radii (Section 8). We close in Section 9 with a discussion of our findings of cluster-scale substructure properties and the implications of our results for dark matter micro-physics.

2. OBSERVED CLUSTER SUB-SAMPLE

In this work, we focus on the study of three massive galaxy clusters that span $z = 0.39\text{--}0.54$, drawn from the observed *HST Frontier Fields* (Lotz 2013) and CLASH (Balestra et al. 2016) programs. As listed in Table 1, this sub-sample was chosen for the publicly available extensive ground-based spectroscopic follow-up data and hence has some of the best constrained mass models at present:

- MACS J0416.1-2403: appears dynamically relaxed (Postman et al. 2012). We adopt the LENSTOOL-optimized cluster lensing model from the *HST Frontier Fields Initiative data* (Lotz et al. 2017; Natarajan et al. 2017b) and independently identify cluster members using the CLASH galaxy catalog (see Chiang et al. 2025a for details).
- MACS J1206.2-0847: appears to be a relaxed, cool core cluster (Ebeling et al. 2009; Postman et al. 2012; Girardi et al. 2015). We adopt the LENSTOOL-optimized lensing model of Caminha et al. (2017) and again identify cluster members

using the CLASH galaxy catalog (see Chiang et al. 2025a).

- MACS J1149.6+2223: appears dynamically relaxed (Postman et al. 2012; Finney et al. 2018). We adopt the LENSTOOL-optimized lensing model from the *HST Frontier Fields Initiative data* and cross-match cluster member galaxies with spectroscopic information from the SIMBAD database (Wenger et al. 2000).

3. SUMMARY OF CLUSTER LENS MODELING

We briefly describe parametric mass models derived by combining strong- and weak-lensing observations of cluster lenses. This modeling methodology adopts self-similar parametric profiles for cluster members, providing constraints on the structural properties of subhalos hosting cluster member galaxies. Parametric mass models are chosen as they are best suited for direct comparison of lensing-inferred subhalo properties with CDM simulations and their halo catalogs.

The publicly available software package LENSTOOL¹ permits the use of observed lensing signals, including the positions and brightnesses of the multiply-imaged strongly lensed galaxies, as well as the positions and shapes of the weakly lensed background galaxies, to reconstruct the detailed mass distribution in massive lensing clusters. The methods used here are standard and have been in use for over two decades, having been amply tested against multiple independent cosmological simulation suites. A review of these modeling methods, along with their power and limitations, can be found in Natarajan et al. (2024); Kneib & Natarajan (2011). LENSTOOL performs multi-scale Bayesian optimization on joint strong+weak lensing constraints to construct mass distributions modeled as the linear superposition of parametric profiles on a range of scales, as proposed by the conceptual model presented in Natarajan & Kneib (1997); Jullo et al. (2007); Niemiec et al. (2020):

$$\phi_{\text{tot}} = \sum_i \phi_i^{\text{halo}} + \sum_j \phi_j^{\text{subhalo}} + \phi_{\kappa}, \quad (1)$$

where ϕ_i^{halo} represents Mpc-scale halos associated with the smooth large-scale cluster gravitational potentials; ϕ_j^{subhalo} are kpc-scale subhalos associated with cluster member galaxies, and ϕ_{κ} a potential constant external shear field. Further details of the mass modeling are provided in Appendix A.

¹ <https://projets.lam.fr/projects/lenstool/wiki>

Cluster	$\langle z_{\text{spec}} \rangle$	RA [°]	Dec [°]	$M_{200} [\text{M}_\odot]$	$R_{200} [\text{Mpc}]$	$N_{\text{gal}}^{\text{spec}}$	References
MACS J0416	0.3972	64.0381	-24.0675	1.53×10^{15}	2.69	66	(1,2,3)
MACS J1206	0.4398	181.5506	-8.8009	1.37×10^{15}	1.96	152	(4,5,6,7)
MACS J1149	0.5420	177.3990	22.3979	1.27×10^{15}	1.84	144	(3,8)

Table 1. Galaxy cluster sample and (from left to right) the respective mean spectroscopic redshift $\langle z_{\text{spec}} \rangle$, RA (J2000), Dec (J2000), best-fit NFW virial halo mass M_{200} , virial radius R_{200} , concentration c , number of spectroscopically confirmed and LENSTOOL-identified member galaxies $N_{\text{gal}}^{\text{spec}}$, and the references: (1) Balestra et al. (2016), (2) Umetsu et al. (2016), (3) Lotz et al. (2017), (4) Biviano et al. (2023), (5) Biviano et al. (2013), (6) Umetsu et al. (2012), (7) Bergamini et al. (2019), and (8) Grillo et al. (2016).

4. THE TNG-CLUSTER SIMULATION: APT COMPARATOR FOR CLUSTER LENSES

To find the closest redshift- and mass-matched simulated analogs to our cluster sub-sample, here we use the TNG-C simulations², a next-generation extension of the IllustrisTNG project designed specifically to model a large sample of galaxy clusters at high resolution in a fully cosmological context (Nelson et al. 2024). The suite comprises zoom-in magnetohydrodynamical simulations of 352 massive galaxy clusters over the mass range $M_{200} = 10^{14\text{--}15.5} \text{ M}_\odot$, run with the moving-mesh code AREPO (Springel 2010) and the full IllustrisTNG galaxy formation model (Pillepich et al. 2018); wherein subhalos are located by SUBFIND (Springel et al. 2001). To preserve the large-scale cosmological environments, target clusters are selected from large dark-matter-only parent boxes and then re-simulated at higher resolution, reaching a fixed dark matter (baryon) particle mass resolution of 6.1×10^7 (1.2×10^7) M_\odot and a gravitational softening length of 1.48 kpc.

In addition to the primary aim of studying the baryon cycle in clusters (ICM thermodynamics, metal enrichment, cool cores/non-cool cores), the TNG-C suite is also ideal for mass-matched comparisons with massive cluster lenses and their substructure demographics. This suite provides the first robust CDM predictions, with fully coupled baryonic physics, for subhalo mass functions, their inner density profiles, and tidal truncation radii in massive galaxy clusters, against which the lensing-inferred properties of observed massive clusters can be calibrated and directly compared.

To select the most representative simulated analogs, we search in the closest redshift-matched data outputs of our sub-sample—MACS J0416 (Snapshot #72), MACS J1206 (Snapshot #70), and MACS J1149 (Snapshot #65)—and find the five best mass-matched systems per cluster, giving $\Delta M_{200}/M_{200} = 0.010\text{--}0.089$ at the end. To self-consistently model the observational selection functions in assigning subhalos, we use the mem-

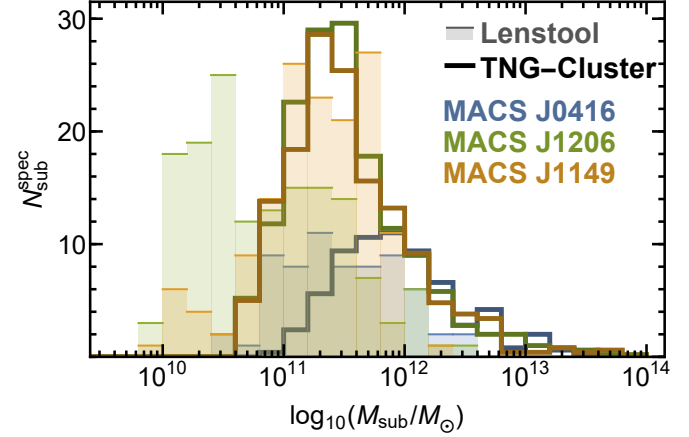


Figure 1. The mass function of subhalos associated with spectroscopically confirmed bright cluster member galaxies in observed lensing clusters (LENSTOOL, color-shaded) compared with CDM predictions from simulated analogs (TNG-Cluster, solid lines) under the same selection criteria; see Section 4 for details.

ber galaxy properties associated with all bound subhalos of a simulated cluster, apply the respective V -band apparent magnitude cuts at corresponding redshifts ($m_V = 27.1\text{--}18.7$ for MACS J0416; $m_V = 26.4\text{--}14.9$ for MACS J1206; $m_V = 22.0\text{--}16.7$ for MACS J1149), and select the subhalos hosting the $N_{\text{gal}}^{\text{spec}}$ -brightest member galaxies as the spectroscopically confirmed analogs³. Such selected subhalos in simulated cluster analogs are found to produce galaxy luminosity functions consistent with the respective observed distributions. Hence, the simulated analogs comprise the same number of subhalos as deployed in each observed cluster lens mass model (Table 1) and provide the best-fit combined mass distribution of both large and small-scale components.

5. SUBHALO MASS FUNCTION

Structure assembles hierarchically in CDM, as smaller halos merge to form more massive structures at later

² <https://www.tng-project.org/cluster/>

³ We have explicitly verified that the results presented in this work remain unchanged under alternative subhalo-mass-based selection criteria for assigning subhalo analogs.

times. The mass function of substructures is a robust prediction of the model, with a power-law slope of $dn/dM_{\text{sub}} \propto M_{\text{sub}}^{-1.9}$ (e.g. van den Bosch & Jiang 2016). The subhalo mass function (SHMF) inside collapsed structures with masses corresponding to a total mass akin to those of observed cluster-lenses $M_{200} \sim 10^{15} M_{\odot}$ can be computed directly from the simulated analogs. In this work, as noted above, we partition the total mass of a cluster into large-scale mass components and smaller scale subhalos that are associated with bright cluster member galaxies.

Fig. 1 compares the SHMFs associated with spectroscopically confirmed member galaxies of each observed clusters and of simulated analogs (averaged over five best-matched systems per cluster). We note reasonably good agreement between the lensing derived ones with CDM predictions, except for MACS J1206 where simulations cannot account for the low-mass end of the observed bi-modal distribution. We contribute this mismatch to the fact that, even in the TNG-C volume, we do not find an analog of MACS J1206 that appears as strongly elongated within the central ~ 200 kpc in projection (e.g, Caminha et al. 2017).

6. SUBSTRUCTURE RADIAL DISTRIBUTION

We next examine the consistency of projected spatial distribution, for each cluster in our sub-sample, between subhalos associated with observed member galaxies and simulated analogs. The top panel of Fig. 2 compares the projected radial distribution of subhalos in observed clusters and in TNG-C analogs. Across all three systems, there is a persistent and stark inconsistency between observations and simulations, where the latter exhibits a dearth of substructures at small projected halo-centric radii $R/R_{200} \lesssim 0.2$ and instead appears to have a roughly radius-independent distribution. To further illustrate this discrepancy, the bottom panels of Fig. 2 compare the projected 2D distributions of observations and simulations. We observe that the simulated cluster analogs fail to reproduce not only the abundance but also the spatial clustering of these substructures at small projected halo-centric radii.

The stark dearth of inner substructures in simulated CDM clusters was first hinted in the analysis of the cluster Cl 0024+16 of Natarajan et al. (2009), and formally codified in Natarajan et al. (2017a) with the subsequent detailed analysis of three additional *HST Frontier Fields* clusters. Beyond the possibility of posing a new tension to the CDM paradigm, the authors noted that this discrepancy could also be partly caused by inaccurate numerical modeling of dynamical friction and tidal stripping or limited accuracy in the subhalo finding algo-

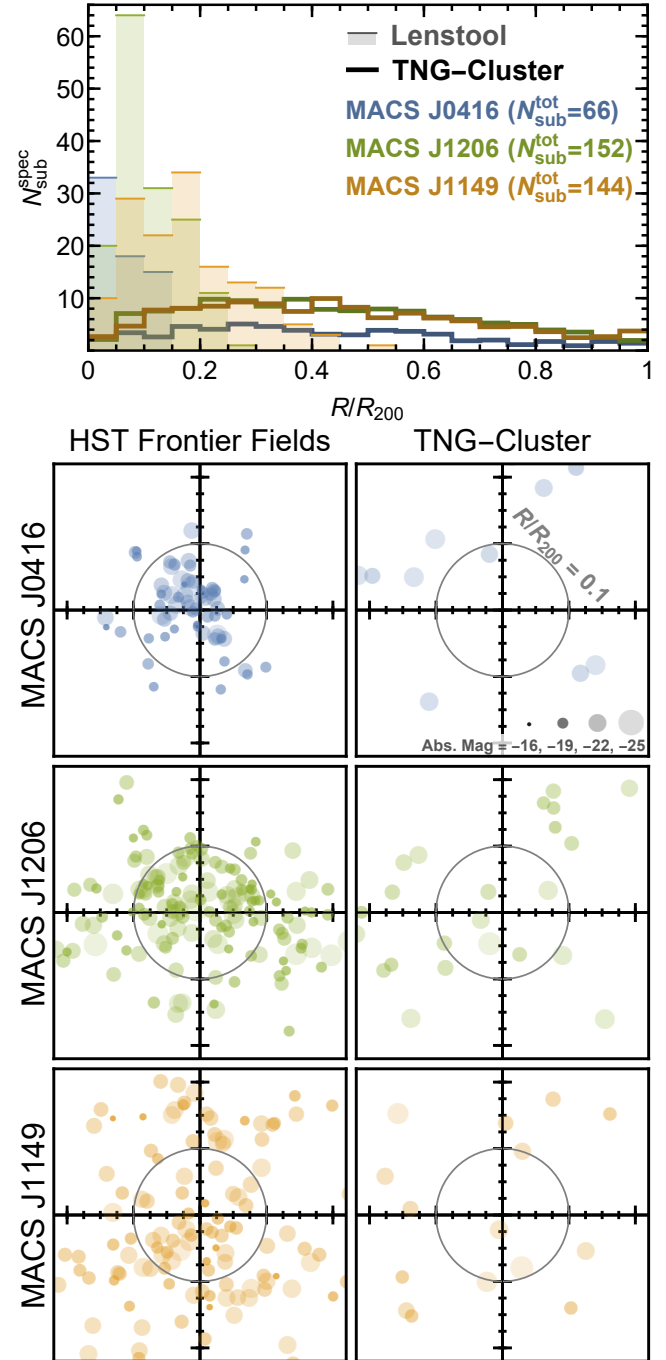


Figure 2. **Top panel:** The projected radial distribution of subhalos associated with spectroscopically confirmed member galaxies in observed clusters (color-shaded) and in simulated analogs (solid lines; averaged over five best-matched analogs and over three random projections). **Bottom panels:** The projected spatial distribution of subhalos around cluster centers in observations (left column) and simulated analogs (right column; from the best mass-matched analog along a random projection), annotated by the respective V -band absolute magnitude of associated galaxies. As compared to observations, simulated analogs clearly show a dearth of, and fail to reproduce the spatial clustering, of inner substructures within $R/R_{200} \lesssim 0.2$.

rithm, leading to artificial reduction of inner substructures in simulated clusters.

Recently, Chiang et al. (2025c) demonstrate that, in state-of-the-art cosmological simulations with kpc-scale force resolution, subhalos with orbital peri-center distances $\lesssim 0.2R_{200}$ are nearly all force-unresolved, leading to artificially enhanced tidal mass loss and run-away disruption (van den Bosch & Ogiya 2018). In parallel, recent halo-finder comparison studies by Mansfield et al. (2024) and Forouhar Moreno et al. (2025) have demonstrated that conventional subhalo finders that rely only on spatial clustering of particles, such as SUBFIND used in TNG-C suite here, are particularly prone to lose track of subhalos at small peri-centers, an issue that can be greatly improved by additionally accessing velocity space information or tracking particles across simulation outputs.

Indeed, when inspecting the 3D halo-centric distances of these simulated subhalos, we find that the number counts are roughly constant between 0.3 – $1R_{200}$ but drop precipitously with decreasing radii below $\lesssim 0.3R_{200}$. Furthermore, when averaging over all simulated cluster analogs, only 10 simulated subhalos lie within a 3D radius of $\leq 0.2R_{200}$ under the luminosity-based selection, which is an order of magnitude smaller than $N_{\text{tot}}^{\text{spec}} \sim 100$ in observed clusters. While numerical resolution artifacts and subhalo finding algorithms undoubtedly contribute to this glaring mismatch, it is unclear and still left to be demonstrated whether CDM predictions, with these numerical uncertainties appropriately addressed, can still adequately reproduce the observed spatial distribution of substructures. Aside from the discrepant abundance, the observed inner substructures also show greater diversity in (V -band) luminosity and more complex projected spatial clustering than the simulated counterparts.

7. THE INNER DENSITY PROFILES OF SUBSTRUCTURES

Galaxy-Galaxy Strong Lensing (GGSL) in massive clusters, as amply demonstrated by Meneghetti et al. (2020a, 2023) offers a uniquely sensitive probe of the abundance and internal structure of dark matter subhalos in the mass range $M_{\text{sub}} \sim 10^{10}$ – $10^{12} M_{\odot}$. GGSL events are a proxy for how efficiently cluster member galaxies, embedded in the smooth cluster potential, generate additional (galaxy-scale) strong-lensing regions beyond those produced by the cluster-scale critical curves alone. These regions appear as *tangential* critical curves in the image plane and map to galaxy-scale caustics on the source plane, thereby delineating where a back-

ground source would be multiply imaged by substructure.

Operationally, the GGSL cross section $\sigma_{\text{GGSL}}(z_s)$ is defined as the total area on the source plane at redshift z_s enclosed by the full set of galaxy-scale caustics. In practice, one identifies the *tangential* critical curves via the lensing Jacobian eigenvalues, maps these curves to the source plane to obtain caustics, and then computes the area covered by the union of the resulting caustics. The corresponding GGSL probability is

$$P_{\text{GGSL}}(z_s) \equiv \frac{\sigma_{\text{GGSL}}(z_s)}{A_s}, \quad (2)$$

where A_s is the source-plane area mapped by the observational field of view (Meneghetti et al. 2020a). With this definition, $P_{\text{GGSL}}(z_s)$ can be interpreted as the fraction of the observed field within which a source at z_s is expected to undergo galaxy-scale strong lensing by cluster substructure.

Using high-fidelity lens models of *HST Frontier Fields* and CLASH clusters, Meneghetti et al. (2020a) showed that the observed GGSL probability exceeds predictions from state-of-the-art hydrodynamical CDM simulations by more than an order of magnitude across a broad range of source redshifts. Subsequent studies (e.g. Ragagnin et al. 2022; Heinze et al. 2024; Meneghetti et al. 2023) confirmed that this tension persists even after varying numerical resolution; subgrid feedback; and line-of-sight projection of simulated clusters. While such effects can alter P_{GGSL} by factors of a few at most, they do not bridge the discrepancy without simultaneously degrading agreement with other independent observables (e.g., the stellar mass function, galaxy sizes, or cluster lensing on larger scales). Importantly, the lensing-inferred subhalo mass functions in these clusters remain broadly consistent with CDM expectations (Natarajan et al. 2017b; Dutra et al. 2025) as discussed in Section 1 and shown in Fig. 1 above, indicating that the GGSL tension is not primarily driven by *subhalo abundance*. Instead, it points to a mismatch to the subhalo *inner structure*: cluster member galaxies appear to reside in subhalos that are systematically more centrally concentrated than in collisionless CDM simulations, enabling them to reach lensing criticality and generate the observed GGSL.

Two recent papers have delved more systematically and deeply into addressing this discrepancy: work by Tokayer et al. (2024), that exhausts the freedom available within collisionless CDM (including extreme but physically motivated baryonic contractions), and by Dutra et al. (2025), who demonstrate that gravothermal core collapse in self-interacting dark matter (SIDM) subhalos might naturally produce the inner density profile slopes required to match the observed GGSL signal.

7.1. Rearranging Mass within Λ CDM: Limits of Baryonic Solutions

Tokayer et al. (2024) revisit the GGSL discrepancy using a subset of five well-studied clusters (AS1063, MACS J0416, MACS J1206, Abell 2744, and PSZ1 G311) with high-quality parametric strong-lensing mass models constructed with LENSTOOL⁴. Recomputing the GGSL probabilities $P_{\text{GGSL}}(z_s)$ using an independent ray-tracing pipeline based on LENSTRONOMY, they confirmed the original Meneghetti et al. (2020a) result.

The central question addressed by Tokayer et al. (2024) is whether, within the standard CDM paradigm including baryons, there exists sufficient freedom in the *radial mass distribution* of galaxy-scale subhalos to reconcile simulations with observations, subject to the constraint that lensing robustly measures the *aperture mass* within a truncation radius r_t for each subhalo. In other words: if one holds the enclosed mass within r_t fixed and consistent with the output of lensing models, can redistributing mass within r_t boost the GGSL probability enough to match the data?

This question is explored in two steps. First, each galaxy-scale dPIE subhalo in the LENSTOOL models is replaced with a truncated NFW (tNFW) profile that reproduces the same mass within r_t , while imposing the usual NFW inner cusp $\rho \propto r^{-1}$ expected in collisionless CDM halos. This transformation preserves the lensing-constrained aperture mass but changes the detailed inner density profile. Ray-tracing the resulting tNFW models yields GGSL probabilities that remain consistent with Meneghetti et al. (2020b), still discrepant with CDM simulations. This leads to the conclusion that simply enforcing NFW-like cusps under fixed aperture mass cannot modify the galaxy-scale lensing signal enough to solve the problem.

Second, Tokayer et al. (2024) include the dissipative effects of baryons explicitly by adding an exponential stellar component to each subhalo to model the collisional baryonic component in the inner-most regions. The stellar component is characterized by a baryon fraction f_b within r_t and a scale radius $r_d = r_b r_t$, after which the adiabatic contraction model of Gnedin et al. (2004) is applied to compute the response of the dark matter subhalo to the condensed baryons. A wide range of (f_b, r_b) are explored, including extreme, maximally contracted choices that drive as much mass as possible into the innermost kiloparsecs while honoring the observational constraint on the total mass enclosed within r_t .

⁴ MACS J0416 and MACS J1206 are also part of the sample analyzed in this work.

Even in the most aggressively baryon-dominated scenarios, the inner log-slope of the total density profile $\gamma \equiv -d \ln \rho / d \ln r$ was found to saturate at $\gamma \lesssim 2$ on GGSL-relevant scales, in agreement with Heinze et al. (2024). The resulting enhancement of the GGSL probability is modest, at most a factor of a few, leaving the discrepancy intact.

In summary, Tokayer et al. (2024) demonstrate that no rearrangement of mass into NFW-like or baryon-contracted profiles that is consistent with collisionless CDM and realistic stellar distributions can reproduce the observed GGSL probabilities. The GGSL discrepancy, therefore, cannot be attributed to missing baryonic physics within the standard CDM framework; it points instead to a genuine shortcoming of collisionless dark matter in reproducing the inner structure of cluster subhalos.

7.2. Gravothermal Core Collapse in SIDM as a Resolution?

Building on this sharpened tension, Dutra et al. (2025) ask what kind of dark matter microphysics could plausibly produce the subhalo inner density profiles implied by the GGSL data. They first independently confirm the robustness of the discrepancy by recalculating GGSL probabilities for the *HST Frontier Fields* clusters plus PSZ1 G311, using both parametric lens models and direct ray-tracing through the underlying particle distributions of mass-matched IllustrisTNG analogs (Nelson et al. 2019). They further show that including realistic ellipticities for the subhalo population and projection effects for the entire cluster changes the GGSL probabilities at the $\lesssim 40\%$ level, still far short of the order-of-magnitude enhancement required.

To connect the GGSL signal to dark matter microphysics, Dutra et al. (2025) adopt a generalized NFW (gNFW) profile for cluster subhalos,

$$\rho(r) = \frac{\rho_s}{(r/r_s)^\gamma \left[1 + (r/r_s)^2\right]^{(\beta-\gamma)/2}}, \quad (3)$$

where γ and β denote the inner and outer logarithmic slopes, respectively. They fix the total mass and large-scale NFW cluster halo, and vary γ while keeping β near the CDM value. This procedure isolates the impact of steepening the inner density profile at fixed subhalo mass and truncation radius, as expected when SIDM subhalos undergo gravothermal core collapse in dense cluster environments (e.g. Balberg et al. 2002; Yang & Yu 2021).

By ray-tracing through clusters in which each galaxy-scale subhalo is modeled as a gNFW profile with a fixed inner log-slope γ , Dutra et al. (2025) quantify how

P_{GGSL} responds to changes in inner structure. They find a strong, monotonic dependence: steepening the cusp from the CDM-like value $\gamma = 1.0$ to $\gamma = 1.5$ increases the GGSL probability by $\sim 1.5\times$, $\gamma = 2.0$ by $\sim 2\times$, $\gamma = 2.5$ by $\sim 3.5\times$, and $\gamma \approx 2.9$, approaching the fully core-collapsed SIDM regime, by $\sim 8\times$, bringing simulations substantially closer to the observed cluster sample. Steepening from $\gamma = 1$ to $\gamma \simeq 2.9$ also implies a dramatic rise in the central density by ~ 4 orders of magnitude within $0.1 r_{200}$, consistent with expectations for deeply core-collapsed SIDM subhalos in high-density environments.

[Dutra et al. \(2025\)](#) then carefully assess whether additional known baryonic processes could generate such steep inner profiles in collisionless CDM. They consider dark-matter spikes around supermassive black holes ([Gondolo & Silk 1999](#)), and “mound” configurations in which black hole feedback compresses the inner halo ([Bertone et al. 2025](#)). While these mechanisms can steepen the dark matter distribution on parsec scales locally, none produces generic $\gamma \gtrsim 2.5$ slopes on the kiloparsec scales probed by GGSL in cluster subhalos, at the required abundance and with realistic black hole and stellar masses. Combined with the explicit baryonic experiments of [Tokayer et al. \(2024\)](#), yet again, this effectively rules out a solution that relies solely on rearranging baryons within an otherwise collisionless CDM framework.

In contrast, SIDM models with sufficiently large, velocity-dependent self-interaction cross sections $\sigma_{\text{SIDM}}/m_{\text{SIDM}}$ naturally exhibit a diversity of inner slopes, including steep, post-core-collapse halos with $\gamma \sim 2.5\text{--}3$ in the densest environments (e.g. [Balberg et al. 2002](#); [Yang & Yu 2021](#)). In such models, lower-density systems (e.g., field dwarfs) may still exhibit cored profiles, while cluster subhalos that have experienced many dynamical times in a high-density background undergo gravothermal collapse and become highly centrally concentrated. The GGSL statistics, therefore, select precisely the regime where SIDM core collapse is expected to operate most efficiently. [Dutra et al. \(2025\)](#) demonstrate that mapping these SIDM-inspired profiles onto subhalos reconciles the observed and simulated GGSL probabilities while preserving the broader, large-scale successes of CDM.

Taken together, the findings of [Tokayer et al. \(2024\)](#) and [Dutra et al. \(2025\)](#) can be used to transform the GGSL discrepancy into a sharp statement about dark matter microphysics. The amplitude of the observed GGSL signal demands galaxy-scale subhalos with inner density slopes $\gamma \gtrsim 2.5$ on kpc scales embedded in cluster lenses. Within collisionless CDM, even extreme

baryon-induced contractions saturate at $\gamma \lesssim 2$ and fail to boost P_{GGSL} by more than a factor of a few. SIDM models that undergo gravothermal core collapse, by contrast, naturally produce the required steep inner profiles in dense environments. The GGSL discrepancy thus cannot be resolved by any plausible rearrangement of mass in collisionless CDM; it instead points toward self-interactions in the dark sector as a compelling extension beyond the standard cosmological paradigm.

8. OUTER-HALO CONSTRAINTS FROM CLUSTER SUBHALO TRUNCATION RADII

[Chiang et al. \(2025a\)](#) explore an orthogonal, outer-halo diagnostic of dark matter microphysics by exploiting the tidal truncation radii of galaxy-scale subhalos in massive clusters inferred from high-fidelity strong+weak lensing mass models. The key result is that the *observed* spatial extents of subhalos in eight clusters are statistically fully consistent with expectations for collisionless CDM, while being in strong tension with the compact truncation radii predicted in the strongly collisional SIDM regime required to drive gravothermal core collapse in cluster subhalos (e.g. [Dutra et al. 2025](#); [Tokayer et al. 2024](#)).

The analysis proceeds in three stages. First, [Chiang et al. \(2025a\)](#) analyze LENSTOOL-optimized the parametric lens models for a sample of eight well-studied clusters (Abell 2218, 383, 963, 209, 2390 and the sub-sample introduced in Section 2), constructed in accord to Section 3. The total mass distribution of each cluster is decomposed into cluster-scale halos plus smaller-scale subhalos that host spectroscopically confirmed cluster member galaxies, all modeled as dual pseudo-isothermal (dPIE) profiles. Empirical luminosity-based scaling relations that tie velocity dispersion, core radius, and truncation radius across the subhalo population are re-optimized for each cluster, so that the lensing-inferred dPIE truncation radius, $r_{t,\text{dPIE}}$, can be used as a directly measured proxy for the subhalo tidal extent.

Second, [Chiang et al. \(2025a\)](#) derive ensemble-level predictions for CDM subhalo truncation radii. Analytically, the tidal radius $r_{t,i}^{\text{CDM}}$ of subhalo i is obtained by equating the mean enclosed density of the subhalo at some fraction $\epsilon_i r_{t,i}^{\text{CDM}}$ to the mean density of the host cluster at the subhalo pericenter radius $r_{\text{per},i}$, following the classical density-matching criterion of [Ghigna et al. \(1998\)](#) and [Taylor & Babul \(2001\)](#):

$$\langle \rho_{\text{gal},i}(\epsilon_i r_{t,i}^{\text{CDM}}) \rangle \simeq \langle \rho_{\text{cluster}}(r_{\text{per},i}) \rangle. \quad (4)$$

The order-unity pre-factor ϵ_i encapsulates the physical scatters sourced by diverse subhalo formation times, orbits, and internal anisotropies. [Chiang et al. \(2025a\)](#)

self-consistently measure the empirical calibration factor $\epsilon_i \equiv r_{t,i}^{\text{dPIE}}/r_{t,i}^{\text{CDM}}$ from subhalos in the range $M_{\text{sub}} = 10^{10.5-12.5} M_{\odot}$ selected from redshift- and mass-matched cluster analogs from the TNG-C suite. Crucially, because the calibration is performed by matching two *definitions* of tidal radius (a density-based definition versus the dPIE truncation radius), it is largely insensitive to numerical resolution-limited artifacts. The central 97% distribution of ϵ_i lies within $\epsilon_i \simeq 0.25-1.18$, with a median $\tilde{\epsilon} \simeq 0.48$. This physical scatter also implies that the analytic truncation estimates are accurate on the *ensemble* level but of limited use on an object-by-object basis.

Third, Chiang et al. (2025a) similarly compute the SIDM subhalo truncation radii in the *strongly collisional* regime relevant for gravothermal core collapse, in which ram-pressure stripping of the subhalo outskirts dominates over collisionless tidal stripping. The truncation radius is estimated by balancing ram pressure from the host with the internal pressure support of the subhalo (Furlanetto & Loeb 2002):

$$\rho_{\text{gal},i}(r_{t,i}^{\text{SIDM}}) \sigma_{\text{gal},i}^2 \simeq \rho_{\text{cluster}}(r_{\text{per},i}) v_{\text{per},i}^2, \quad (5)$$

which generically predicts significantly more compact tidal radii than the CDM density-matching prescription. Observationally, only projected cluster-centric distances R_{gal} and line-of-sight velocities v_{los} are measured. Chiang et al. (2025a) therefore construct conservative CDM and SIDM estimates in terms of $(R_{\text{gal}}, v_{\text{los}})$, ultimately adopting

$$r_{t,i}^{\text{SIDM}} = \min(r_{t,i}^{\text{CDM}}, r_{t,i}^{\text{ram}}) \quad (6)$$

as a conservative *upper bound* on the SIDM truncation radius.

Applying this calibrated framework to a total of 418 subhalo hosting spectroscopically confirmed member galaxies from the eight independent clusters, Chiang et al. (2025a) compare lensing-derived subhalo truncation radii r_t^{obs} with CDM and SIDM predictions, as summarized in Fig. 3. Across all clusters, the CDM distribution is statistically consistent with the observed truncation radii over the full range of galaxy luminosities (equivalently, $\sigma_{\text{gal}}/\sigma_{\text{gal},*}$). This agreement holds cluster-by-cluster despite heterogeneous data quality, works of independent modeling teams, and a range of cluster dynamical states.

In stark contrast, the SIDM predictions for the strongly collisional regime needed to induce gravothermal core collapse in cluster subhalos fall one to two orders of magnitude *below* the lensing-inferred tidal radii in every cluster. Because $r_{t,i}^{\text{SIDM}}$ serves as conservative upper bounds given $v_{\text{los}} \leq v_{\text{per}}$, any realistic SIDM

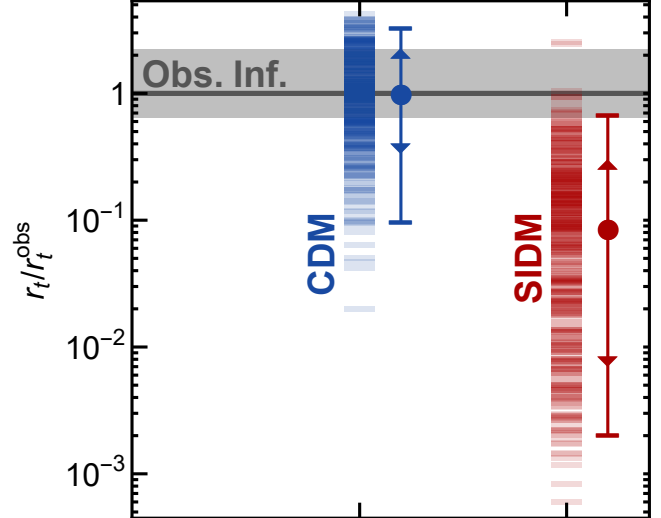


Figure 3. Tidal radii from lensing-based observational inferences (gray line; shading indicates conservative 5σ uncertainties), overlaid with individual CDM (blue horizon dashes) and strongly collisional SIDM (red; conservative upper bounds) predictions over a sample of 418 spectroscopically confirmed member galaxies across eight massive clusters (Abell 2218, 383, 963, 209, 2390, and MACS J0416, J1206, J1149). We also plot the respective median (circles), central 68% (triangles), and central 95% ranges (horizontal bars). Lensing inferences are fully statistically consistent with CDM and discrepant with SIDM.

model with $\sigma_{\text{SIDM}}/m_{\text{SIDM}} \gtrsim \text{few cm}^2 \text{g}^{-1}$ on cluster-subhalo velocity scales would yield even more compact truncation radii than shown. The discrepancy between these compact SIDM tidal radii and the observationally inferred truncation radii cannot be bridged by projection effects, orbital uncertainties, or by the calibrated factor-of-few scatter in ϵ_i ; the entire core-collapsing SIDM family of distributions lies well outside the observational 5σ band.

Chiang et al. (2025a) therefore conclude that in the mass range $M_{\text{sub}}^{\text{dPIE}} \simeq 5 \times 10^9-10^{12} M_{\odot}$ that primarily contributes to GGSL, the outer structure of cluster subhalos is fully consistent with *collisionless* tidal stripping, and that any strongly collisional SIDM model capable of driving core collapse in cluster subhalos is robustly excluded. Rather than quote a single exclusion value for $\sigma_{\text{SIDM}}/m_{\text{SIDM}}$, they emphasize that the mapping between truncation radius and cross section is highly non-linear and depends on unknown pericenter velocities and assembly histories, and that the factor of $\sim 4-5$ scatter in ϵ_i precludes object-level constraints. The appropriate interpretation is therefore at the ensemble-level: cluster subhalos in these violent environments behave as if dark matter self-interactions are negligible, consistent with and complementary to independent upper limits from

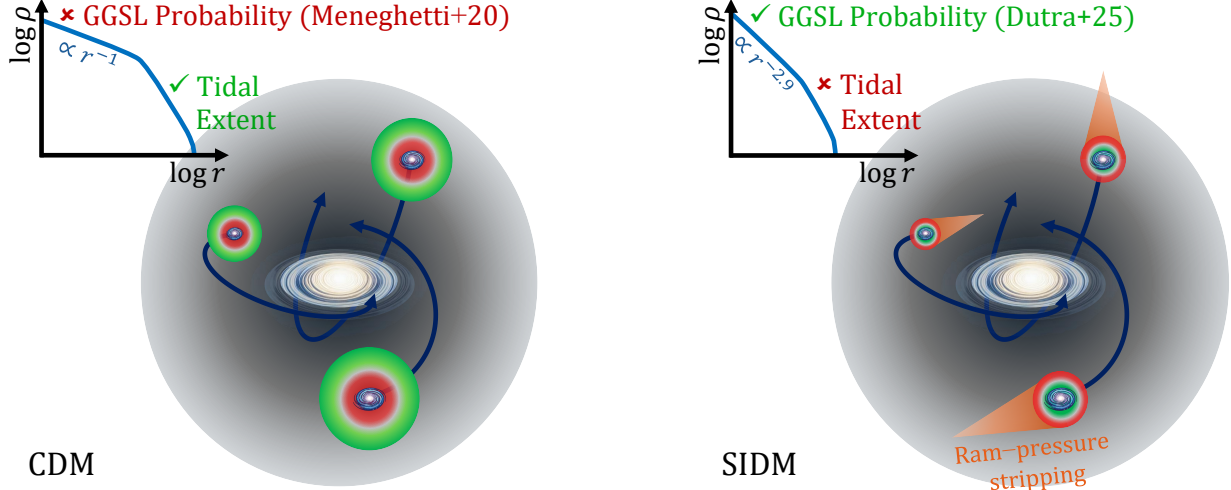


Figure 4. Schematic illustrating the implications for CDM and SIDM models. **Left panel:** Collisionless CDM matches subhalo tidal extents but severely under-predicts GGSL. **Right panel:** Core-collapsed SIDM yields steep inner profiles that match GGSL, but this strongly collisional regime also results in more pronounced mass stripping that significantly reduces tidal extents even after accounting for the slight expansion of the outskirts due to outward energy transfer during core collapsing. The inset axes show the run of $\log \rho$ versus $\log r$ (not to scale).

cluster mergers and dwarf-galaxy kinematics (e.g. Yang & Yu 2021). In concert with the GGSL-based *inner-halo* constraints from Tokayer et al. (2024) and Dutra et al. (2025), these results sharpen the emerging picture in which the outer structure of cluster subhalos is CDM-like, while any SIDM resolution of the GGSL tension must invoke finely tuned, strongly velocity-dependent or resonant cross sections that are suppressed on cluster-subhalo scales.

To briefly summarize the two distinct regimes of cluster subhalos explored in Sections 7 and 8, weak- and strong-lensing reconstructions isolate two robust facts about cluster subhalos, as illustrated in Fig. 4. First, at large radii ($r \gtrsim 50$ kpc) their tidal extents and outskirts are consistent with collisionless CDM (left panel) (Chiang et al. 2025a). Second, the observed GGSL probability demands much steeper inner density slopes, $\gamma \gtrsim 2.5$ within $r \lesssim 10$ kpc, than those produced by CDM with baryons alone (right panel) (Meneghetti et al. 2020a, 2022; Dutra et al. 2025; Tokayer et al. 2024). Constant-cross-section SIDM can boost the GGSL rate via core collapse in the inner regions, but if collisional nature persists throughout the halo, it tends to over-strip subhalos and shrink tidal radii. Meanwhile, velocity-dependent SIDM generally yields smoother radial trends tied to dispersion rather than a sharp spatial transition. If CDM is to be modified, these findings motivate a new picture in which self-interactions are *inactive* in the outskirts and *active* in dense cores. This can be accomplished either by invoking entirely new dark matter physics or through a hybrid dark matter model that includes a combination of CDM and SIDM.

9. CONCLUSIONS & DISCUSSION

Stress-testing key substructure properties in observed lensing clusters with their simulated CDM analogs from the TNG-C suite, we find intriguing results showing that not all current observational constraints can be accounted for by collisionless dark matter. Our findings from four physical diagnostics are summarized below:

- **Subhalo mass functions:** Reasonably good statistical agreement is found between the SHMFs derived from cluster lenses and those from simulated CDM TNG-C clusters.
- **Outer subhalo structure:** Lensing-inferred subhalo tidal truncation radii are in excellent agreement with collisionless CDM, ruling out any additional sizable contribution of self-interaction-induced mass loss on these scales of ~ 5 –10 kpc.
- **Inner subhalo structure:** The high efficiency of observed GGSL requires significantly concentrated subhalo inner mass distributions with steeper-than-NFW central profiles, which are naturally produced only in the core-collapse regime of SIDM.
- **Radial distribution of subhalos:** The projected spatial distribution of inner substructures in observed massive clusters is highly discrepant with CDM. Simulated subhalos do not appear to adequately populate in the inner regions $R \leq 0.2 R_{200}$ of clusters, where there is a significant concentration of observed bright cluster galaxies.

Taken together, our results reveal that no single dark matter model currently appears capable of reproducing all aspects of substructure demographics in observed massive clusters self-consistently. Statistically, CDM matches the SHMF and the outer subhalo extents, but cannot account for the inner lensing anomalies. The radial distribution of subhalos also remains highly discrepant, with a marked absence of simulated subhalos at projected cluster-centric radii $R \leq 0.2 R_{200}$. On the flip side, introducing strong self-interactions can account for the observed inner lensing efficiency, but also results in a suppressed SHMF and even stronger depletion of inner substructures relative to CDM due to enhanced tidal mass loss by self-interaction-induced ram pressure stripping and core formation (e.g. Nadler et al. 2020, 2025). Reconciling cluster-scale lensing data across all radii may require hybrid models in which dark matter behaves collisionlessly in the outskirts but exhibits effective self-interaction in the dense cores of subhalos. This dichotomy, we conclude, highlights a critical challenge for the microphysics of dark matter.

For the galaxy-scale lens JVAS B1938+666 at $z_{\text{spec}} = 0.881$, Powell et al. (2025) and Vegetti et al. (2026) claim the detection of a dark, compact $\simeq 10^6 M_{\odot}$ object whose mass profile can be described with a point-mass-like component—potentially arising from core-collapse SIDM, like the inner parts of the subhalos we reported in Dutra et al. (2025)—and an additional extended mass distribution with a radius of 139 pc. This curious detection simply adds to the case we make for core-collapse SIDM.

In this Letter, informed by multi-scale lensing analysis that effectively probes physical scales of 5–10 kpc and substructure properties across multiple independent dense cluster environments, we present a new and fundamental paradox: the incompatibility of the nature of dark matter microphysics required to self-consistently account for the inner and outer properties of cluster subhalos. We demonstrate that while CDM severely under-predicts the lensing efficiency of the inner parts of subhalos constrained by GGSL observations, it can successfully explain the lensing-inferred outer tidal truncation radii of subhalos. This inherent lack of self-consistency is a real crisis for CDM (Fig. 4).

In summary, gravitational lensing offers a powerful, indispensable, and unique probe of dark matter theories. Further stress-testing dark matter models demands new, even higher-resolution cosmological simulations and improved lensing data for larger cluster samples, which are expected imminently from EUCLID and the LSST Rubin Observatory. The anomalies we report here warrant further investigation while robustly pointing the way to potentially new dark matter theories.

¹ P.N. gratefully acknowledges funding from the Department of Energy grant DE-SC001766; support from the John Templeton Foundation via grant 126613 and from the NASA GLIMPSE JWST GO-03293.026 for this work. ² I.D. acknowledges support from NASA under award No. 80NSSC25K0311 under the NASA FINESST program.

REFERENCES

Balberg, S., Shapiro, S. L., & Inagaki, S. 2002, *The Astrophysical Journal*, 568, 475, doi: [10.1086/339038](https://doi.org/10.1086/339038)

Balestra, I., Mercurio, A., Sartoris, B., et al. 2016, *Astrophys. J. Suppl.*, 224, 33, doi: [10.3847/0067-0049/224/2/33](https://doi.org/10.3847/0067-0049/224/2/33)

Bergamini, P., Rosati, P., Mercurio, A., et al. 2019, *Astron. Astrophys.*, 631, A130, doi: [10.1051/0004-6361/201935974](https://doi.org/10.1051/0004-6361/201935974)

Bertone, G., Wierda, A. R. A. C., Gaggero, D., et al. 2025, *PhRvD*, 112, 043537, doi: [10.1103/5nnf-8fz9](https://doi.org/10.1103/5nnf-8fz9)

Biviano, A., et al. 2013, *Astron. Astrophys.*, 558, A1, doi: [10.1051/0004-6361/201321955](https://doi.org/10.1051/0004-6361/201321955)

Biviano, A., Pizzuti, L., Mercurio, A., et al. 2023, *ApJ*, 958, 148, doi: [10.3847/1538-4357/acf832](https://doi.org/10.3847/1538-4357/acf832)

Bullock, J. S., & Boylan-Kolchin, M. 2017, *Annual Review of Astronomy and Astrophysics*, 55, 343, doi: [10.1146/annurev-astro-091916-055313](https://doi.org/10.1146/annurev-astro-091916-055313)

Caminha, G. B., Grillo, C., Rosati, P., et al. 2017, *A&A*, 607, A93, doi: [10.1051/0004-6361/201731498](https://doi.org/10.1051/0004-6361/201731498)

Chiang, B. T., Dutra, I., & Natarajan, P. 2025a, *arXiv e-prints*, arXiv:2511.14726, doi: [10.48550/arXiv.2511.14726](https://doi.org/10.48550/arXiv.2511.14726)

Chiang, B. T., van den Bosch, F. C., & Schive, H.-Y. 2025b, *MNRAS*, 544, 36, doi: [10.1093/mnras/staf1639](https://doi.org/10.1093/mnras/staf1639)

—. 2025c, *arXiv e-prints*, arXiv:2510.26901, doi: [10.48550/arXiv.2510.26901](https://doi.org/10.48550/arXiv.2510.26901)

Cruz, A., Brooks, A., Lisanti, M., et al. 2025, *arXiv e-prints*, arXiv:2510.11800, doi: [10.48550/arXiv.2510.11800](https://doi.org/10.48550/arXiv.2510.11800)

Del Popolo, A., & Le Delliou, M. 2017, *Galaxies*, 5, 17, doi: [10.3390/galaxies5010017](https://doi.org/10.3390/galaxies5010017)

Dutra, I., Natarajan, P., & Gilman, D. 2025, *The Astrophysical Journal*, 978, 38, doi: [10.3847/1538-4357/ad9b09](https://doi.org/10.3847/1538-4357/ad9b09)

Ebeling, H., Ma, C. J., Kneib, J. P., et al. 2009, MNRAS, 395, 1213, doi: [10.1111/j.1365-2966.2009.14502.x](https://doi.org/10.1111/j.1365-2966.2009.14502.x)

Elíasdóttir, Á., Limousin, M., Richard, J., et al. 2007, arXiv e-prints, arXiv:0710.5636, doi: [10.48550/arXiv.0710.5636](https://doi.org/10.48550/arXiv.0710.5636)

Faber, S. M., & Jackson, R. E. 1976, ApJ, 204, 668, doi: [10.1086/154215](https://doi.org/10.1086/154215)

Finney, E. Q., Bradač, M., Huang, K.-H., et al. 2018, Astrophys. J., 859, 58, doi: [10.3847/1538-4357/aabf97](https://doi.org/10.3847/1538-4357/aabf97)

Forouhar Moreno, V. J., Helly, J., McGibbon, R., et al. 2025, MNRAS, 543, 1339, doi: [10.1093/mnras/staf1478](https://doi.org/10.1093/mnras/staf1478)

Furlanetto, S., & Loeb, A. 2002, Astrophys. J., 565, 854, doi: [10.1086/324693](https://doi.org/10.1086/324693)

Ghigna, S., Moore, B., Governato, F., et al. 1998, MNRAS, 300, 146, doi: [10.1046/j.1365-8711.1998.01918.x](https://doi.org/10.1046/j.1365-8711.1998.01918.x)

Girardi, M., et al. 2015, Astron. Astrophys., 579, A4, doi: [10.1051/0004-6361/201425599](https://doi.org/10.1051/0004-6361/201425599)

Gnedin, O. Y., Kravtsov, A. V., Klypin, A. A., & Nagai, D. 2004, Astrophys. J., 616, 16, doi: [10.1086/424914](https://doi.org/10.1086/424914)

Gondolo, P., & Silk, J. 1999, Phys. Rev. Lett., 83, 1719, doi: [10.1103/PhysRevLett.83.1719](https://doi.org/10.1103/PhysRevLett.83.1719)

Grillo, C., Karman, W., Suyu, S. H., et al. 2016, Astrophys. J., 822, 78, doi: [10.3847/0004-637X/822/2/78](https://doi.org/10.3847/0004-637X/822/2/78)

Heinze, F. M., Despali, G., & Klessen, R. S. 2024, MNRAS, 527, 11996, doi: [10.1093/mnras/stad3894](https://doi.org/10.1093/mnras/stad3894)

Jullo, E., Kneib, J.-P., Limousin, M., et al. 2007, New Journal of Physics, 9, 447, doi: [10.1088/1367-2630/9/12/447](https://doi.org/10.1088/1367-2630/9/12/447)

Kneib, J.-P., & Natarajan, P. 2011, A&A Rv, 19, 47, doi: [10.1007/s00159-011-0047-3](https://doi.org/10.1007/s00159-011-0047-3)

Limousin, M. 2024, arXiv e-prints, arXiv:2411.03075, doi: [10.48550/arXiv.2411.03075](https://doi.org/10.48550/arXiv.2411.03075)

Lotz, J. 2013, HST Frontier Fields ("FRONTIER"), STScI/MAST, doi: [10.17909/T9KK5N](https://doi.org/10.17909/T9KK5N)

Lotz, J. M., Koekemoer, A., Coe, D., et al. 2017, ApJ, 837, 97, doi: [10.3847/1538-4357/837/1/97](https://doi.org/10.3847/1538-4357/837/1/97)

Mansfield, P., Darragh-Ford, E., Wang, Y., et al. 2024, ApJ, 970, 178, doi: [10.3847/1538-4357/ad4e33](https://doi.org/10.3847/1538-4357/ad4e33)

Meneghetti, M., Davoli, G., Bergamini, P., et al. 2020a, Science, 369, 1347, doi: [10.1126/science.aax5164](https://doi.org/10.1126/science.aax5164)

Meneghetti, M., et al. 2020b, Science, 369, 1347, doi: [10.1126/science.aax5164](https://doi.org/10.1126/science.aax5164)

Meneghetti, M., Ragagnin, A., Borgani, S., et al. 2022, Astronomy & Astrophysics, 668, A188, doi: [10.1051/0004-6361/202243779](https://doi.org/10.1051/0004-6361/202243779)

Meneghetti, M., Cui, W., Rasia, E., et al. 2023, Astronomy & Astrophysics, 678, L2, doi: [10.1051/0004-6361/202346975](https://doi.org/10.1051/0004-6361/202346975)

Nadler, E. O., Banerjee, A., Adhikari, S., Mao, Y.-Y., & Wechsler, R. H. 2020, ApJ, 896, 112, doi: [10.3847/1538-4357/ab94b0](https://doi.org/10.3847/1538-4357/ab94b0)

Nadler, E. O., Kong, D., Yang, D., & Yu, H.-B. 2025, arXiv e-prints, arXiv:2503.10748, doi: [10.48550/arXiv.2503.10748](https://doi.org/10.48550/arXiv.2503.10748)

Natarajan, P., De Lucia, G., & Springel, V. 2007, MNRAS, 376, 180, doi: [10.1111/j.1365-2966.2007.11399.x](https://doi.org/10.1111/j.1365-2966.2007.11399.x)

Natarajan, P., & Kneib, J.-P. 1997, MNRAS, 287, 833, doi: [10.1093/mnras/287.4.833](https://doi.org/10.1093/mnras/287.4.833)

Natarajan, P., Kneib, J.-P., Smail, I., et al. 2009, ApJ, 693, 970, doi: [10.1088/0004-637X/693/1/970](https://doi.org/10.1088/0004-637X/693/1/970)

Natarajan, P., Loeb, A., Kneib, J.-P., & Smail, I. 2002, Astrophys. J. Lett., 580, L17, doi: [10.1086/345547](https://doi.org/10.1086/345547)

Natarajan, P., & Springel, V. 2004, ApJL, 617, L13, doi: [10.1086/427079](https://doi.org/10.1086/427079)

Natarajan, P., Williams, L. L. R., Bradač, M., et al. 2024, SSRv, 220, 19, doi: [10.1007/s11214-024-01051-8](https://doi.org/10.1007/s11214-024-01051-8)

Natarajan, P., Chadayammuri, U., Jauzac, M., et al. 2017a, MNRAS, 468, 1962, doi: [10.1093/mnras/stw3385](https://doi.org/10.1093/mnras/stw3385)

—. 2017b, MNRAS, 468, 1962, doi: [10.1093/mnras/stw3385](https://doi.org/10.1093/mnras/stw3385)

Nelson, D., Pillepich, A., Ayromlou, M., et al. 2024, A&A, 686, A157, doi: [10.1051/0004-6361/202348608](https://doi.org/10.1051/0004-6361/202348608)

Nelson, D., Springel, V., Pillepich, A., et al. 2019, Computational Astrophysics and Cosmology, 6, 2, doi: [10.1186/s40668-019-0028-x](https://doi.org/10.1186/s40668-019-0028-x)

Niemiec, A., Jauzac, M., Jullo, E., et al. 2020, Monthly Notices of the Royal Astronomical Society, 493, 3331, doi: [10.1093/mnras/staa473](https://doi.org/10.1093/mnras/staa473)

Pillepich, A., Springel, V., Nelson, D., et al. 2018, MNRAS, 473, 4077, doi: [10.1093/mnras/stx2656](https://doi.org/10.1093/mnras/stx2656)

Postman, M., Coe, D., Benítez, N., et al. 2012, Astrophys. J. Suppl., 199, 25, doi: [10.1088/0067-0049/199/2/25](https://doi.org/10.1088/0067-0049/199/2/25)

Powell, D. M., McKean, J. P., Vegetti, S., et al. 2025, Nature Astronomy, 9, 1714, doi: [10.1038/s41550-025-02651-2](https://doi.org/10.1038/s41550-025-02651-2)

Ragagnin, A., et al. 2022, Astron. Astrophys., 665, A16, doi: [10.1051/0004-6361/202243651](https://doi.org/10.1051/0004-6361/202243651)

Sales, L. V., Wetzel, A., & Fattah, A. 2022, Nature Astronomy, 6, 897, doi: [10.1038/s41550-022-01689-w](https://doi.org/10.1038/s41550-022-01689-w)

Schechter, P. 1976, ApJ, 203, 297, doi: [10.1086/154079](https://doi.org/10.1086/154079)

Springel, V. 2010, MNRAS, 401, 791, doi: [10.1111/j.1365-2966.2009.15715.x](https://doi.org/10.1111/j.1365-2966.2009.15715.x)

Springel, V., White, S. D. M., Tormen, G., & Kauffmann, G. 2001, MNRAS, 328, 726, doi: [10.1046/j.1365-8711.2001.04912.x](https://doi.org/10.1046/j.1365-8711.2001.04912.x)

Taylor, J. E., & Babul, A. 2001, ApJ, 559, 716, doi: [10.1086/322276](https://doi.org/10.1086/322276)

Tokayer, Y. M., Dutra, I., Natarajan, P., et al. 2024, The Astrophysical Journal, 970, 143, doi: [10.3847/1538-4357/ad51fd](https://doi.org/10.3847/1538-4357/ad51fd)

Umetsu, K., Zitrin, A., Gruen, D., et al. 2016, ApJ, 821, 116, doi: [10.3847/0004-637X/821/2/116](https://doi.org/10.3847/0004-637X/821/2/116)

Umetsu, K., Medezinski, E., Nonino, M., et al. 2012, *Astrophys. J.*, 755, 56, doi: [10.1088/0004-637X/755/1/56](https://doi.org/10.1088/0004-637X/755/1/56)

van den Bosch, F. C., & Jiang, F. 2016, *MNRAS*, 458, 2870, doi: [10.1093/mnras/stw440](https://doi.org/10.1093/mnras/stw440)

van den Bosch, F. C., & Ogiya, G. 2018, *MNRAS*, 475, 4066, doi: [10.1093/mnras/sty084](https://doi.org/10.1093/mnras/sty084)

Vegetti, S., White, S. D. M., McKean, J. P., et al. 2026, arXiv e-prints, arXiv:2601.02466. <https://arxiv.org/abs/2601.02466>

Wenger, M., Ochsenbein, F., Egret, D., et al. 2000, *A&AS*, 143, 9, doi: [10.1051/aas:2000332](https://doi.org/10.1051/aas:2000332)

Yang, D., & Yu, H.-B. 2021, *PhRvD*, 104, 103031, doi: [10.1103/PhysRevD.104.103031](https://doi.org/10.1103/PhysRevD.104.103031)

APPENDIX

A. LENS MODELING

The larger scale halos as well as the subhalo population is modeled as self-similar dual pseudoisothermal elliptical mass distributions (dPIE) whose 3D density profile ρ_{dPIE} , enclosed mass profile M_{dPIE} , and 2D surface density profile Σ_{dPIE} are given by:

$$\begin{aligned}\rho_{\text{dPIE}}(r) &\equiv \frac{\rho_0}{\left(1 + \frac{r^2}{r_{\text{core}}^2}\right)\left(1 + \frac{r^2}{r_{\text{t}}^2}\right)}, \\ M_{\text{dPIE}}(r) &= 4\pi\rho_0 \left(\frac{r_{\text{core}}^2 r_{\text{t}}^2 \left[r_{\text{t}} \tan^{-1} \left(\frac{r}{r_{\text{t}}} \right) - r_{\text{core}} \tan^{-1} \left(\frac{r}{r_{\text{core}}} \right) \right]}{r_{\text{t}}^2 - r_{\text{core}}^2} \right), \\ \Sigma_{\text{dPIE}}(R) &= \frac{\Sigma_0 r_{\text{core}}}{1 - \left(\frac{r_{\text{core}}}{r_{\text{t}}} \right)} \left(\frac{1}{\sqrt{r_{\text{core}}^2 + R^2}} - \frac{1}{\sqrt{r_{\text{t}}^2 + R^2}} \right),\end{aligned}\quad (\text{A1})$$

where r_{core} denotes the core radius, and r_{t} tidal truncation radius of the subhalo. In this parameterization, the total mass $M_{\text{dPIE}}(r \rightarrow \infty) = 2\pi\Sigma_0 r_{\text{core}} r_{\text{t}}$ is finite.

For each subhalo, the normalization coefficients ρ_0 and Σ_0 are set uniquely by the effective velocity dispersion:

$$\sigma_{\text{dPIE}} \equiv \frac{4G\pi\rho_0}{3} \frac{r_{\text{core}}^2 r_{\text{t}}^3}{(r_{\text{t}} - r_{\text{core}})(r_{\text{t}} + r_{\text{core}})^2} = \frac{4G\Sigma_0}{3} \frac{r_{\text{core}} r_{\text{t}}^2}{r_{\text{t}}^2 - r_{\text{core}}^2}, \quad (\text{A2})$$

where G denotes the gravitational constant. The numerical values of σ_{dPIE} are derived for all substructures simultaneously by optimizing the entire observed cluster lens images. It turns out that σ_{dPIE} is related to the physically measured central velocity dispersion of each member galaxy by $\sigma_{\text{dPIE}}^2 = \frac{2}{3}\sigma_{\text{gal}}^2$ that is available for the member galaxies in the clusters studied here.

With the further assumption that light traces mass on cluster galaxy scales, the free parameters associated with individual subhalos are constrained by the empirical scaling relation of cluster member galaxies (Natarajan et al. 2002; Elíasdóttir et al. 2007; Limousin 2024)

$$\begin{aligned}\sigma_{\text{dPIE}} &= \sigma_{\text{dPIE}*} \left(\frac{L}{L_*} \right)^\alpha, \\ r_{\text{t}} &= r_{\text{t}*} \left(\frac{L}{L_*} \right)^\beta, \\ r_{\text{core}} &= r_{\text{core}*} \left(\frac{L}{L_*} \right)^{1/2},\end{aligned}\quad (\text{A3})$$

where quantities with a star subscript denote the characteristic member galaxy properties, obtained by fitting a Schechter function to the luminosities of the hosted member galaxies (Schechter 1976). The values $\alpha = 0.25$ and $\beta = 0.5$ correspond to the Faber-Jackson relation (Faber & Jackson 1976) are favored for two of the best-fit cluster mass models of our sample, bar MACS J1206 where we find best-fit values of $\alpha = 0.28$ and $\beta = 0.64$ respectively.

As noted above, the total mass of individual substructure scales as $M_{\text{dPIE}}(r \rightarrow \infty) = (9\sigma_{\text{dPIE}*}^2 r_{\text{t}*}^3 / 2G)(L/L_*)^{2\alpha+\beta}$, yielding a mass-to-light ratio that scales as $\Upsilon \propto (L/L_*)^{2\alpha+\beta-1}$. Physically, $2\alpha + \beta = 1$ corresponds to a system with a mass-independent mass-to-light ratio (although possible spatial dependence in Υ is still allowed during the Bayesian optimization); $2\alpha + \beta > 1$ indicates that brighter member galaxies exhibit larger Υ .